Supporting Information

Tetranitro- and Tetraamino- dibenzo[18]crown-6-ether Derivatives: Complexes for Alkali Metal Ions, Redox Potentials, Crystal Structures, Molecular Sorption, and Proton Conducting Behaviours

Yuta Shimizu,[a] Takashi Takeda,[a, b]* Norihisa Hoshino,[a, b] and Tomoyuki Akutagawa [a, b]*

[a] Graduate School of Engineering, Tohoku University, Sendai 980-8579, Japan and [b] Institute of Multidisciplinary Research for Advanced Materials (IMRAM), Tohoku University, 2-1-1 Katahira, Aoba-ku, Sendai 980-8577, Japan.

Institute of Multidisciplinary Research for Advanced Materials (IMRAM), Tohoku University, 2-1-1 Katahira, Aoba-ku, Sendai 980-8577, Japan

Phone: +81-22-217-5653

Fax: +81-22-217-5655

E-mail akutagawa@tohoku.ac.jp

Contents

Experimental section

Physical measurements.

UV-vis-NIR and IR spectra were recorded using PerkinElmer Lambda 750 and Thermo Fisher Scientific Nicolet 6700 FT-IR spectrophotometers, respectively. Thermogravimetric (TG) analysis and differential scanning calorimetry (DSC) analysis were conducted using a Rigaku Thermo plus TG8120 thermal analysis station and a Mettler DSC1-T with an Al_2O_3 reference and a heating and cooling rate of 5 K min^{-1} under a nitrogen atmosphere. The *T*-dependent dielectric constants were measured using the two-probe AC impedance method from 100 Hz to 1 MHz (Hewlett-Packard, HP4194A) and the temperature controller of a Linkam LTS-E350 system. The electrical contacts were prepared using gold paste (Tokuriki 8560) to attach 25-μm ϕ gold wires to the 3-mm ϕ compressed pellet, as well as 10-μm ϕ gold wires to each single crystal.

Preparation.

Crown ethers **1** and **2** were prepared using the methods stated in the literature.[59] Yellow-colored single-crystals of **1**·2CH_3CN were obtained via the slow evaporation of the crystallization solvent of CH_3CN; this was obtained using **1** (9.80 mg, 18.1 μmol) and LiI (3.65 mg, 27.3 μmol) in boiling CH_3CN (3 mL). White-needle single-crystals of **2**·0.33H_2O were obtained by the recrystallization of **2** from boiling CH_3OH in the presence of hydrated hydrazine.

Orange-colored block-shaped single-crystals of [Na(**1**)I]·3CH_3CN were obtained via the slow evaporation of CH_3CN (10 mL) dissolved in **1** (23.5 mg, 43.4 μmol) and NaI (20.7 mg, 138 μmol). Yellow-colored block-shaped single-crystals of [K(**1**)I]·4CH_3CN were obtained via the slow evaporation of the crystallized CH_3CN (10 mL) dissolved in **1** (20.6 mg, 38.1 μmol) and KI (20.2 mg, 122 μmol). Yellow-colored block-shaped single-crystals of [Rb(**1**)I]·3CH_3CN were obtained via the slow evaporation of boiling CH_3CN (10 mL) dissolved in **1** (20.3 mg, 37.6 μmol) and RbI (29.2 mg, 138 μmol). Yellow-colored block-shaped single-crystals of (Cs^+•**1**)•I^- were prepared via slow evaporation of boiling CH_3CN (10 mL) dissolved in **1** (20.2 mg, 37.4 μmol) and CsI (20.6 mg, 79.4 μmol).

Red needle-shaped single-crystals of [Na(**2**)$(H_2SO_4)_3$]·nH_2O were prepared by mixing **2** (20.5 mg, 48.8 μmol) and NaI (24.4 mg, 163 μmol) in dilute H_2SO_4 (1.64 M, 6 mL); the solution was subjected to two-phase diffusion at 281 K using CH_3OH. Red needle-shaped single-crystals of [K(**2**)$(H_2SO_4)_3$]·nH_2O were obtained by mixing **2** (69.9 mg, 166 μmol) and KI (75.1 mg, 452 μmol) in a dilute H_2SO_4 solution (1.64 mol/L, 20 mL), which was placed in the two-phase diffusion crystallization environment of CH_3OH at 281 K. Elemental analysis: Calc. for $C_{20}H_{43}N_4Na_{0.25}O_{22.5}S_3$ {[$(Na^+)_{0.25}$(**2**)$(H_2SO_4)_3$] · 4.5H_2O}: C, 29.97; H, 5.41; N, 6.99. Found: C, 29.88; H, 5.42; N, 6.85. Calc. for $C_{20}H_{48}KN_4O_{25}S_3$ {[$(K^+)_{0.25}$(**2**)$(H_2SO_4)_3$]·7H_2O}: C, 27.30; H, 5.50; N, 6.37. Found: C, 27.54; H, 5.37; N, 6.38.

Structural determination of crystals.

Single crystals were obtained using a slow-cooling method. Crystallographic data were collected using a Rigaku RAPID-II diffractometer equipped with a rotating anode fitted with multilayer confocal optics and Cu Kα (λ = 1.54187 Å) radiation from a graphite monochromator at T = 100 K. Structural refinements were performed using the full-matrix least-squares method on F^2. Calculations were performed using Crystal Structure software packages. All parameters (except for those of the hydrogen atoms), were refined using anisotropic temperature factors. Table 1 summarizes the crystal data and parameters.

Theoretical calculations.

Density functional theory (DFT) calculations of **1**, **2**, H_2**2**$^{2+}$, and the related molecules were performed using the Gaussian 16 program package. The optimized molecular structures were obtained via DFT calculations based on the B3LYP/6-31G (d, p) basis set.

Table S1. Crystal data, data collection, and reduction parameters of **1** and **2**.

Crystal	**1**·2CH_3CN	[Na(**1**)I]·3CH_3CN	[K(**1**)I]·4CH_3CN	[Rb(**1**)I]·3CH_3CN
Formula	$C_{22}H_{23}N_5O_{14}$	$C_{26}H_{31}N_7O_{14}NaI$	$C_{26}H_{31}N_7O_{14}KI$	$C_{26}H_{29}RbIN_7O_{14}$
Formula weight	581.45	815.46	870.61	875.93
Space group	*Pnma* (#62)	*Pbca* (#61)	*Pca*2_1 (#29)	*P*-1 (#2)
a, Å	7.5672(3)	17.6971(3)	18.5633(3)	10.6237(3)
b, Å	22.2189(8)	18.6927(3)	9.31515(17)	11.2609(4)
c, Å	15.2555(6)	20.9582(4)	21.2695(4)	15.1068(5)
α, deg	–	–	–	88.389(6)
β, deg	–	–	–	82.391(6)
γ, deg	–	–	–	74.364(5)
V, Å^3	2564.97(18)	6933.1(2)	3677.91(12)	1725.01(11)
Z	4	8	4	2
D_{calc}, g·cm^{-3}	1.511	1.562	1.572	1.686
μ, cm^{-1}	11.131	80.387	85.157	96.568
Reflections measured	26379	73769	39737	18919
Independent reflections	2407	6336	6663	6167
Reflections used	2407	6336	6663	6167
R_{int}	0.0726	0.1081	0.0503	0.0961
R_1 [a]	0.0620	0.0638	0.0506	0.0572
R_{all}	0.0926	0.0844	0.0642	0.0707
$R_w(F_2)$ [a]	0.2290	0.1443	0.1469	0.0961
GOF	0.837	1.039	1.095	1.073
CCDC	2168847	2168842	2168840	2168843

Crystal	[Cs(**1**)I]	**2**·0.33H_2O	[Na(**2**)$(H_2SO_4)_3$]·6H_2O	[K(**2**)$(H_2SO_4)_3$]·4(H_2O)
Chemical formula	$C_{20}H_{20}CsIN_4O_{14}$	$C_{20}H_{28}N_4O_{6.33}$	$C_{40}H_{80}N_8NaO_{42.5}S_6$	$C_{20}H_{21}KN_4O_{22}S_3$
Formula weight	800.21	425.74	1568.45	796.68
Space group	$P2_1/n$ (#14)	$P2_1$ (#4)	$Pca2_1$ (#29)	$Pna2_1$ (#33)
a, Å	9.15319(17)	16.8353(4)	34.7439(9)	11.1964(2)
b, Å	17.8073(3)	8.4802(2)	8.1437(2)	16.8470(4)
c, Å	16.9471(3)	23.1290(6)	23.0281(6)	19.1707(4)
α, deg	–	–	–	–
β, deg	105.200(7)	110.799(8)	–	–
γ, deg	–	–	–	–
V, Å^3	2665.63(13)	3086.9(2)	6515.6(3)	3616.10(13)
Z	4	6	4	4
D_{calc}, g·cm^{-3}	1.994	1.374	1.599	1.463
μ, cm^{-1}	206.212	8.636	30.052	36.931
Reflections measured	28791	34844	71878	40108
Independent reflections	4823	9990	11887	6508
Reflections used	4823	9990	11887	6508
R_{int}	0.1501	0.0338	0.0774	0.0354
R_1 [a]	0.0554	0.0709	0.1115	0.0819
R_{all}	0.0683	0.0980	0.1533	0.0957
$R_w(F_2)$ [a]	0.1174	0.2302	0.3417	0.2570
GOF	1.066	1.060	1.175	1.047
CCDC	216884	2168845	2168846	2168844

[a] $R = \Sigma||F_o| - |F_c|| / \Sigma|F_o|$ and $R_w = (\Sigma\omega(|F_o| - |F_c|)^2 / \Sigma\omega F_o^2)^{1/2}$.

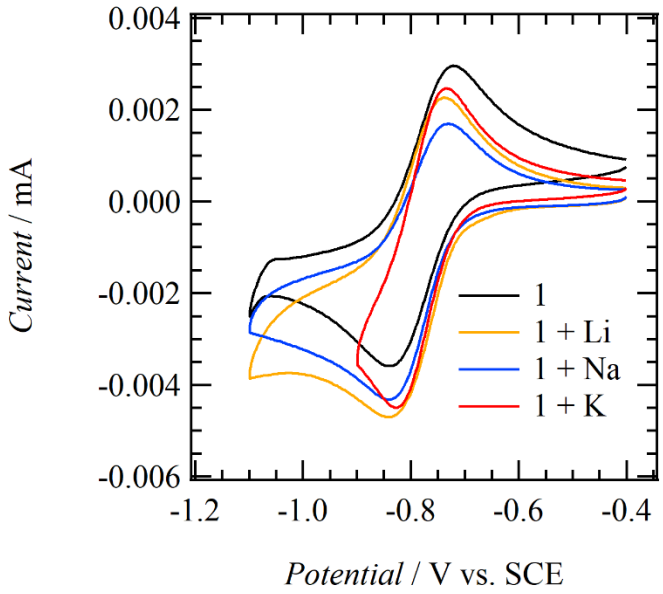

Figure S1. CV charts of **1** under the existence of 10 molar Li^+, Na^+, and K^+ in DMSO (WE: GC, CE: Pt, Supporting electrolyte: $TBABF_4$ (0.1 M), Sweep speed: 0.1 V sec^{-1}).

Table S2. Redox potentials of **1** under the existence of 10 molar Li^+, Na^+, and K^+ in DMSO (WE: GC, CE: Pt, Supporting electrolyte: $TBABF_4$ (0.1 M), Sweep speed: 0.1 V sec^{-1}).

	E^{ox} [V]	E^{red} [V]	$E_{1/2}$ [V]	ΔE [mV]
Non	-0.721	-0.839	-0.780	-
Li^+	-0.738	-0.844	-0.791	-11.0
Na^+	-0.731	-0.841	-0.786	-6.0
K^+	-0.734	-0.827	-0.781	-0.5

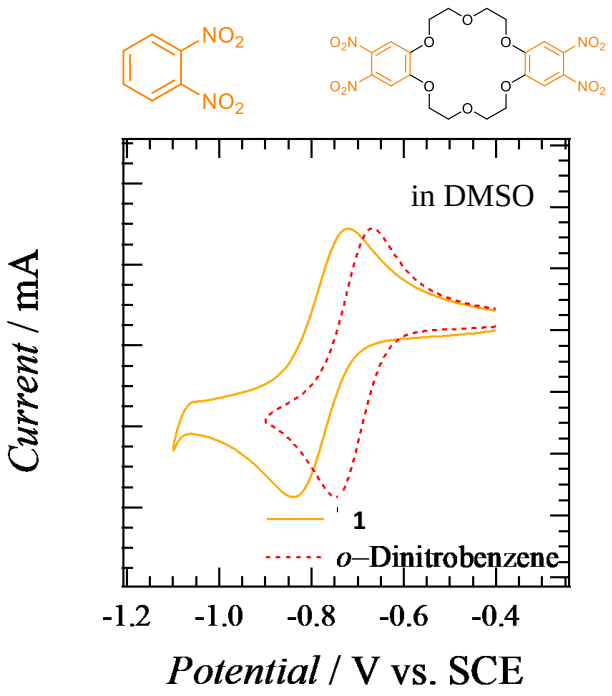

Figure S2. CV charts of **1** and *o*-DNB in DMSO (WE: GC, CE: Pt, Supporting electrolyte: $TBABF_4$ (0.1 M), Sweep speed: 0.1 V sec^{-1}).

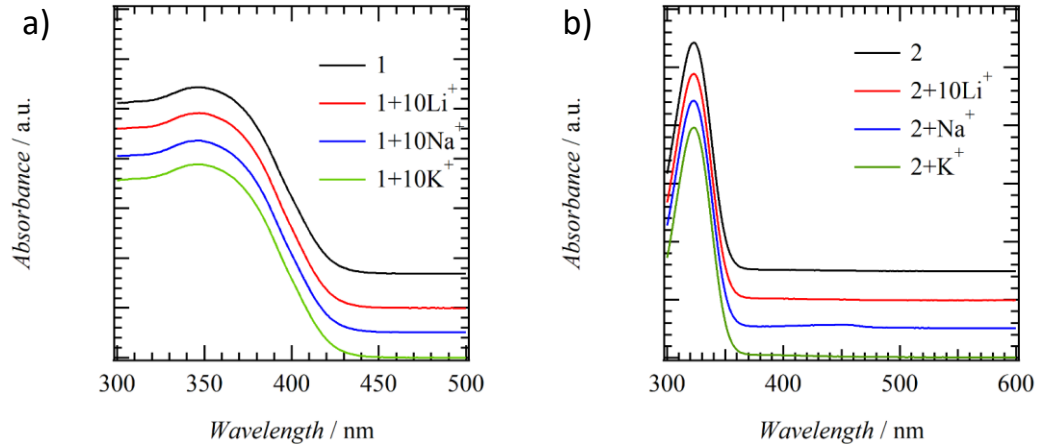

Figure S3. UV-vis spectra of **1** and **2** in DMSO by the additions of 10 molar Li^+, Na^+, and K^+. The baselines were shifted to clarify the spectra.

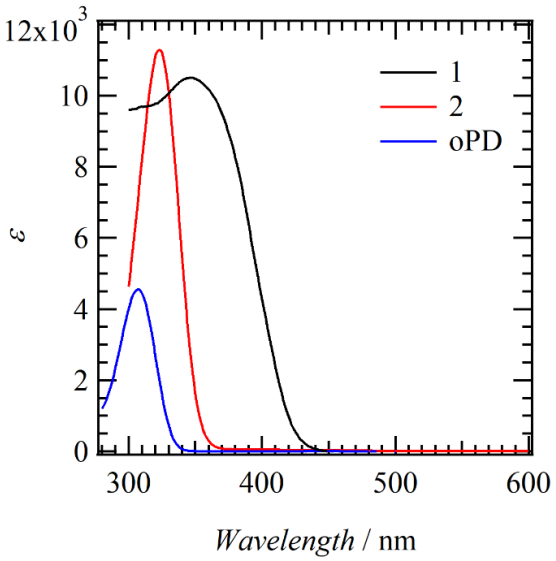

Figure S4. UV-vis spectra of **1**, **2**, and OPD in DMSO.

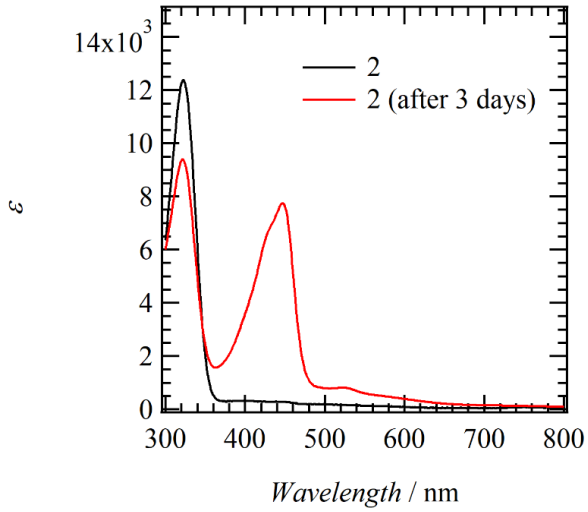

Figure S5. Time-dependent UV-vis spectra of **2** in DMSO.

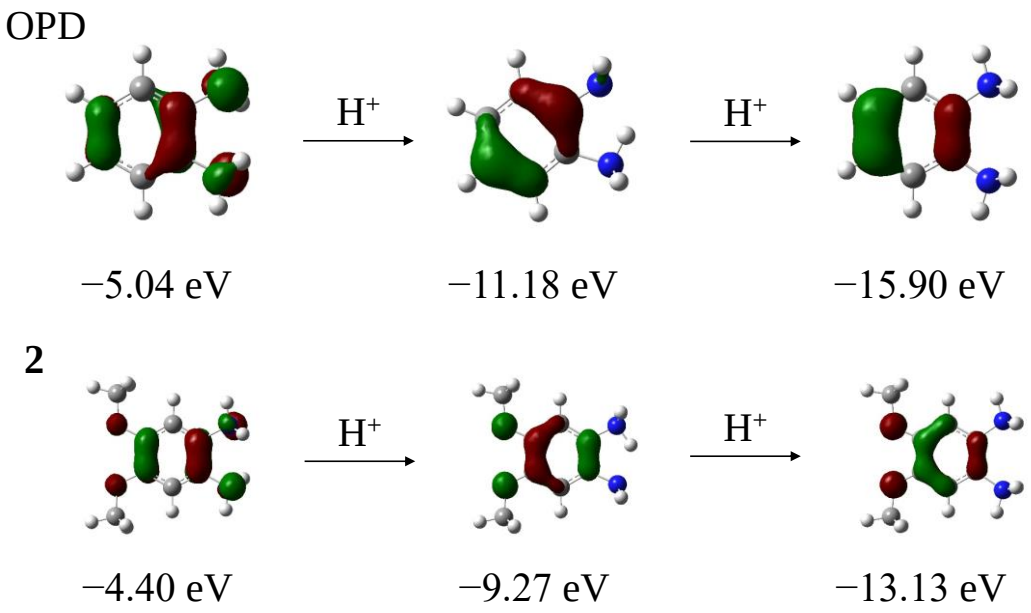

Figure S6. Theoretical calculations of HOMO levels for the protonation of OPD → $HOPD^+$ → $H2OPD^{2+}$ and **2** → $H\mathbf{2}^+$ → $H_2\mathbf{2}^{2+}$.

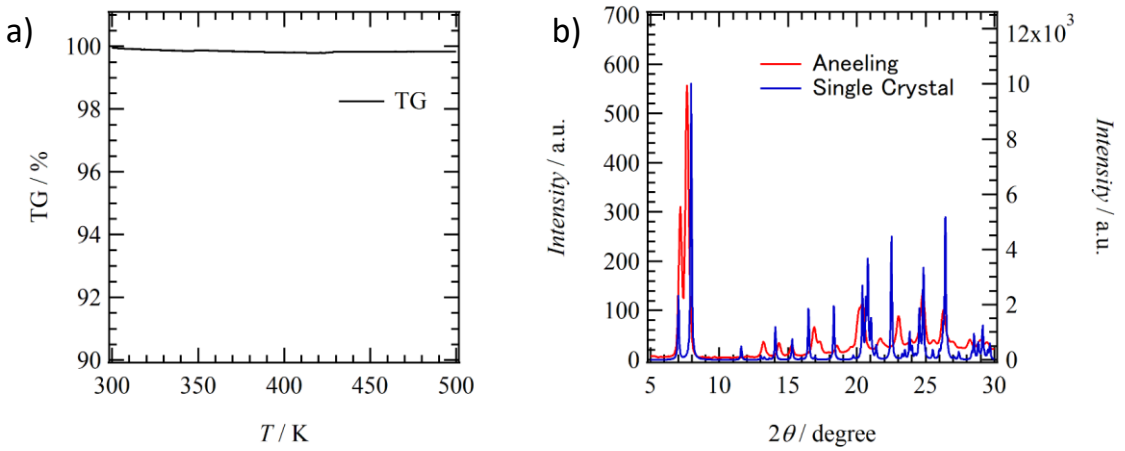

Figure S7. Thermally annealed powder sample of **1**. a) TG chart and b) XRD pattern of annealed powder and simulated pattern of single-crystal X-ray analysis at 100 K.

Table S3. M^+ ~ O distances of M(**1**) structures in [M(**1**)I]·nCH_3CN salts. .

M1~O	M1~O1	M1~O2	M1~O3	M1~O4	M1~O5	M1~O6
Na~O	Na1~O1	Na1~O2	Na1~O3	Na1~O4	Na1~O5	Na1~O6
	2.737(4)	2.726(4)	2.738(4)	2.694(4)	2.597(4)	2.654(4)
K~O	K1~O1	K1~O2	K1~O3	K1~O4	K1~O5	K1~O6
	2.802(4)	2.751(4)	2.844(4)	2.786(5)	2.812(4)	2.865(4)
Rb~O	Rb1~O1	Rb1~O2	Rb1~O3	Rb1~O4	Rb1~O5	Rb1~O6
	3.075(3)	2.898(3)	2.955(3)	3.101(3)	3.039(4)	3.048(3)
Cs~O	Cs1~O1	Cs1~O2	Cs1~O3	Cs1~O4	Cs1~O5	Cs1~O6
	3.255(4)	3.260(5)	3.167(5)	3.301(5)	3.222(6)	3.208(5)

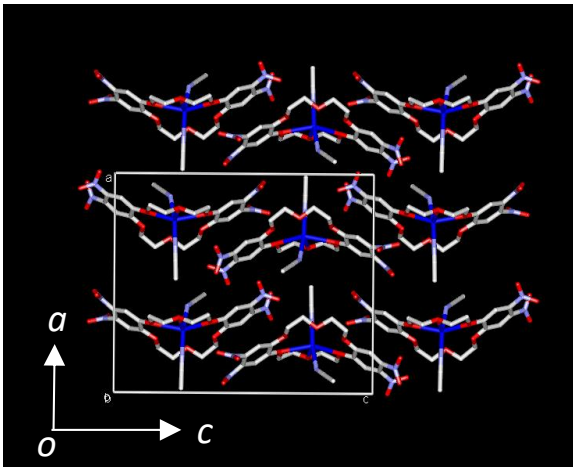

Figure S8. Unit cell of (Na^+•**1**)•2(CH_3CN) viewed along the *b*-axis.

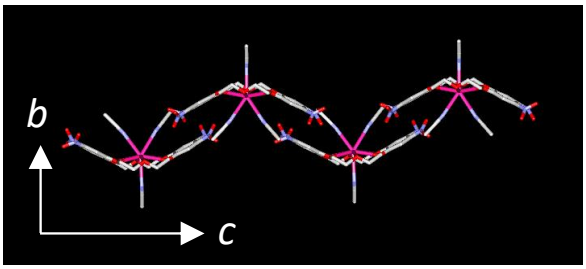

Figure S9. One-dimensional array of (K^+•**1**)•3(CH_3CN) along the *c*-axis.

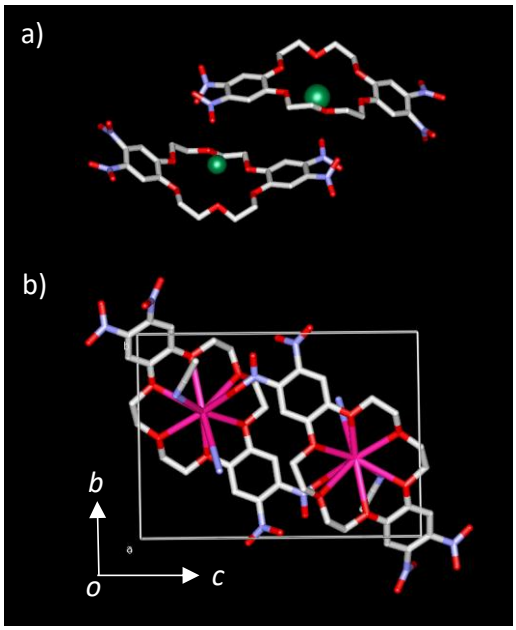

Figure S10. Crystal structure of (Rb^+•**1**)•(CH_3CN). a) Coordination dimer and the unit cell of (Rb^+•**1**)•(CH_3CN) viewed along the *a*-axis.

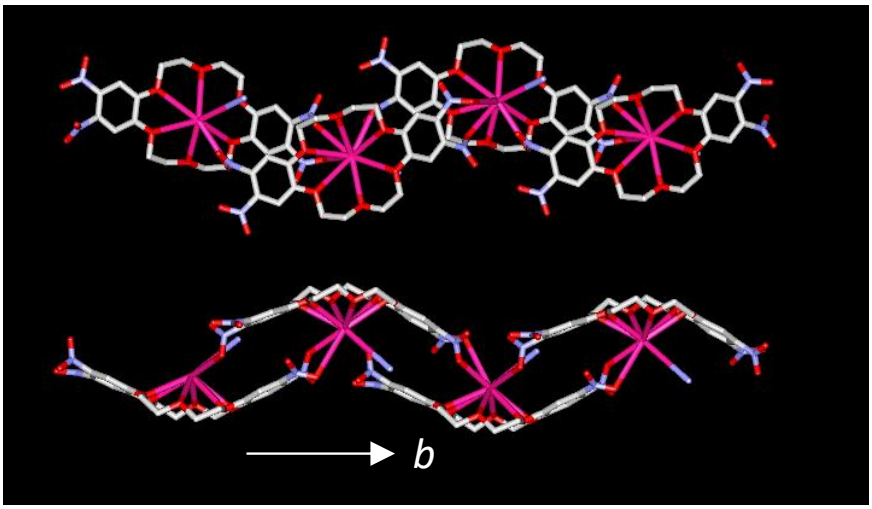

Figure S11. One-dimensional coordination array of (Cs^+•**1**) along the *a*-axis.

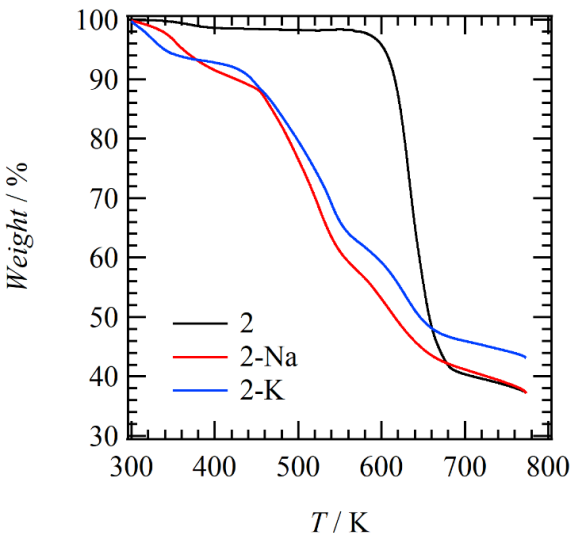

Figure S12. TG charts of **2**, (Na^+•**2**)•(HSO_4^-)$_3$•n(H_2O), and (K^+•**2**)•(HSO_4^-)$_3$•n(H_2O).

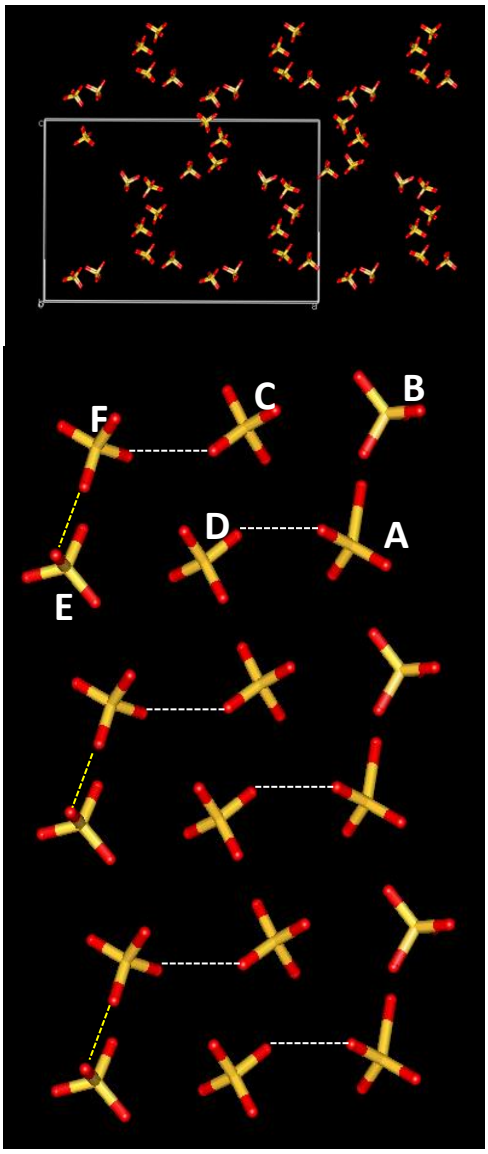

Figure S13. HSO_4^- arrangements in $(Na^+ \bullet \mathbf{2}) \bullet (HSO_4^-)_3 \bullet n(H_2O)$.

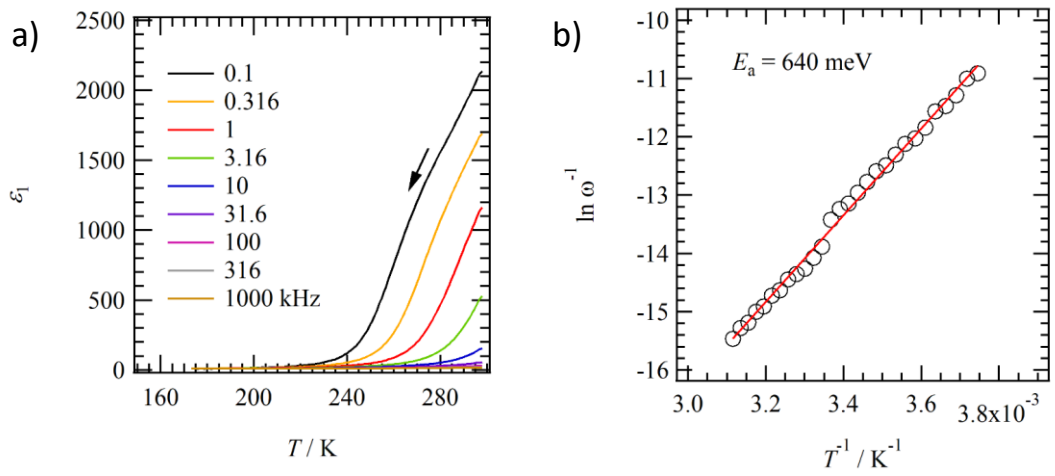

Figure S14. *T*- and *f*-dependent dielectric responses and proton-conducting behavior of $(Na^+)_{0.25}(H_3O^+)_{0.5}(H_2\mathbf{2^{2+}})\bullet(HSO_4^-)_{2.75}(H_2SO_4)_{0.25}\bullet 6(H_2O)$. a) The ε_1 responses of the hydrated crystals. b) Arrhenius plots of *T*- and *f*-dependent ε_2 responses.

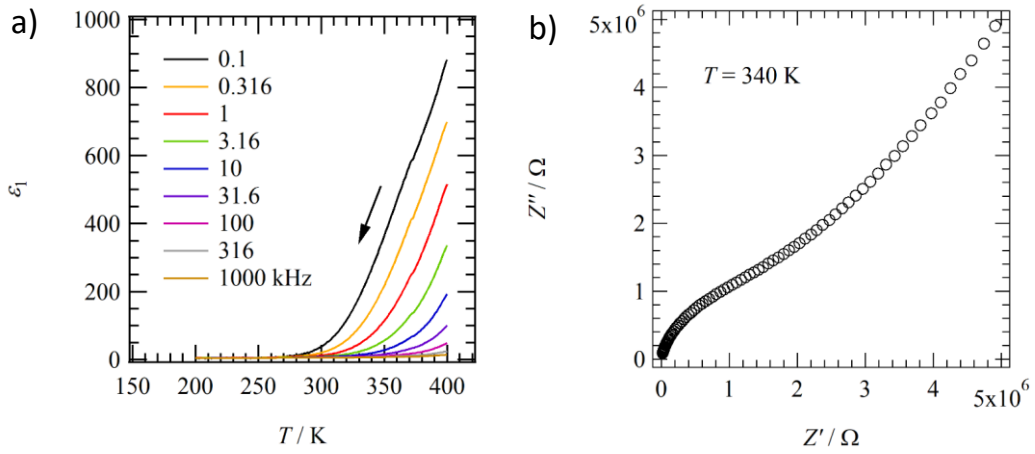

Figure S15. *T*- and *f*-dependent dielectric responses and proton-conducting behavior of dehydrated $(Na^+)_{0.25}(H_3O^+)_{0.5}(H_2\mathbf{2^{2+}})\bullet(HSO_4^-)_{2.75}(H_2SO_4)_{0.25}$. The ε_1 responses of the dehydrated crystals. b) Cole – Cole plot at 340 K.

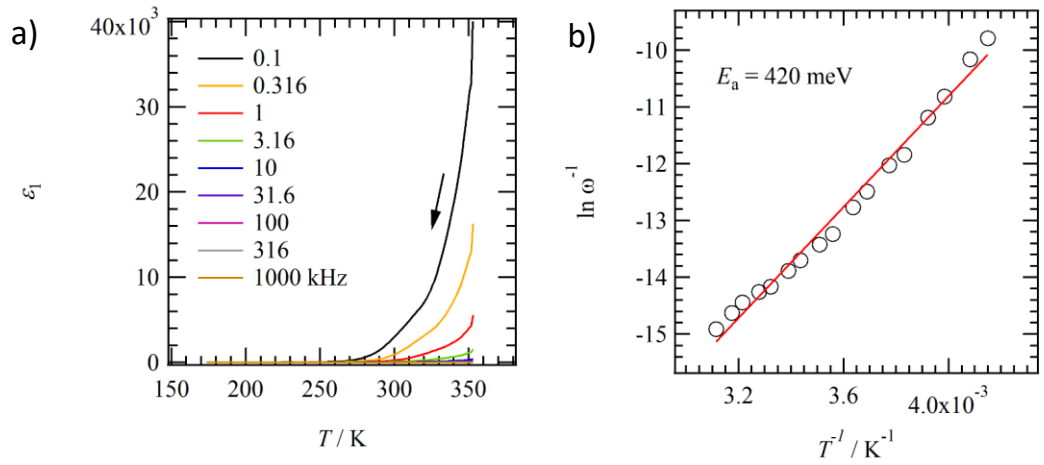

Figure S16. *T*- and *f*-dependent dielectric responses and proton-conducting behavior of $(K^+ \bullet H_2\mathbf{2}^{2+}) \bullet (HSO_4^-)_3 \bullet 4(H_2O)$. a) The ε_1 responses of the hydrated crystals. b) Arrhenius plots of *T*- and *f*-dependent ε_2 responses.

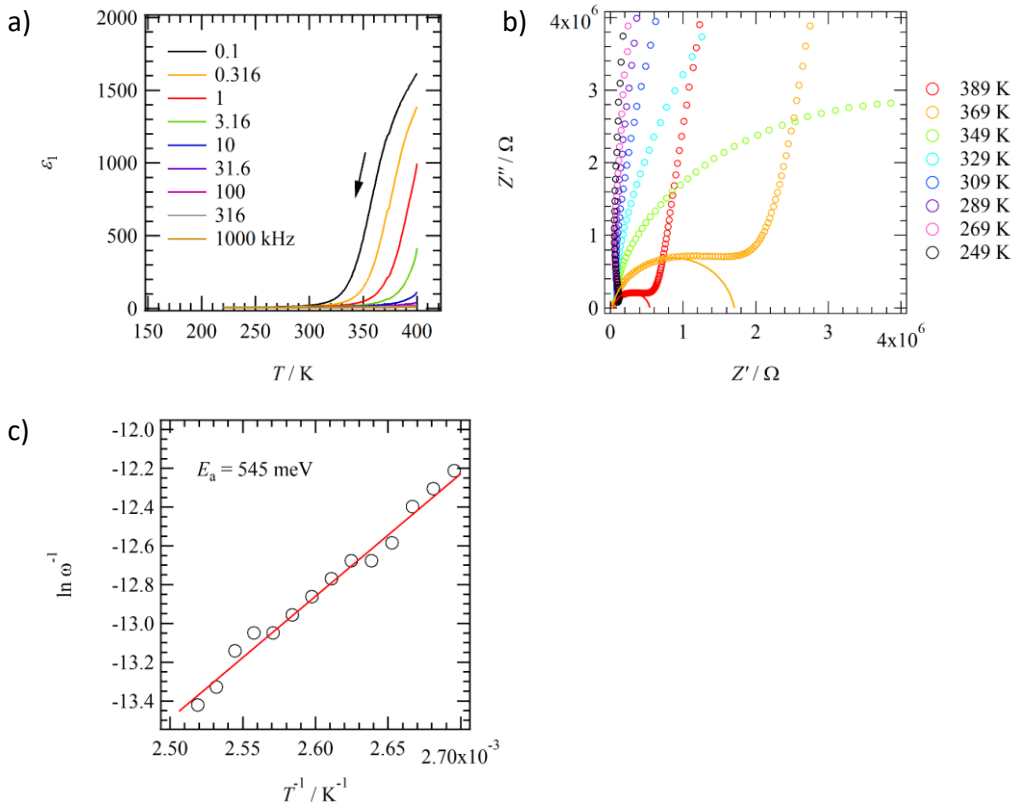

Figure S17. *T*- and *f*-dependent dielectric responses and proton-conducting behavior of dehydrated $(K^+ \bullet H_2\mathbf{2}^{2+}) \bullet (HSO_4^-)_3 \bullet 4(H_2O)$. a) The ε_1 responses of the dehydrated crystals. b) Cole – Cole plot at 340 K. c) Arrhenius plots of *T*- and *f*-dependent ε_2 responses.